Available online at www.sciencedirect.com
ScienceDirect
Journal of Colloid and Interface Science 306 (2007) 459–463
JOURNAL OF Colloid and Interface Science
www.elsevier.com/locate/jcis

Note

Applying grazing incidence X-ray reflectometry (XRR) to characterising nanofilms on mica

Wuge H. Briscoe [a,*,1], Meng Chen [a], Iain E. Dunlop [a,2], Jacob Klein [a,3], Jeffrey Penfold [b], Robert M.J. Jacobs [a,*]

[a] *Physical and Theoretical Chemistry Laboratory, University of Oxford, South Parks Road, Oxford OX1 3QZ, United Kingdom*
[b] *Rutherford Appleton Laboratory, Chilton, Didcot OX11 0QX, United Kingdom*

Received 29 September 2006; accepted 15 October 2006
Available online 21 October 2006

Abstract

Molecularly smooth mica has hitherto not been widely used as a substrate for the X-ray reflectometry (XRR) technique. That is largely due to the difficulty of achieving flatness over a sufficiently large area of mica. Here we show that this difficulty can be overcome by slightly bending the mica substrate over an underlying cylinder; the enhanced rigidity of the bent mica sheet along the axis of the cylinder provides sufficient flatness along this axis for XRR measurements. To test this method, we have employed it to characterise three types of nanofilms on mica in air: (A) Cr–Au thin films; (B) a surface-grown zwitterionic polymer brush; and (C) a Langmuir–Blodgett (LB) phospholipid monolayer, using a table-top X-ray reflectometer. Fitting the obtained reflectivity curves with the standard Parratt algorithm allows us to extract the structural information of the nanofilms (both thickness and apparent roughness). Our simple method points to how XRR may be exploited as a useful characterisation tool for nanofilms on mica.

Keywords: XRR; Thin films; Nanofilms; X-ray reflectometry; Mica; Surface-grown polymer brushes; Surface characterisation

1. Introduction

Polymers and amphiphilic molecules (e.g., surfactants or lipids) can be attached onto solid surfaces to form films of nanometer thickness, as an effective strategy to modify surface properties and to mediate desirable surface interactions. The efficacy of such processes hinges on our ability to tailor, and thus on our understanding of, the structures of these soft nanofilms. There are a range of optical methods that are available to unravel such structural information, such as ellipsometry and Fourier transform infrared spectroscopy (FTIR). Due to its readily achievable molecular smoothness, mica is the preferred model substrate in many techniques such as the surface force apparatus/balance (SFA/B) [1–3] and the atomic force microscope (AFM) [4], as well as the electron microscope (EM) [5]. Techniques to probe the corresponding structure of the mica-surface-adsorbed films would be highly complementary to such force or imaging methods. However, due to mica's intrinsic birefringence, the optical characterisation methods routinely employed for other substrates such as silicon, silica, quartz and sapphire have not been widely applied to nanofilms on mica [6]. This is partly because reliable data is hard to obtain, as the optical axes of the mica substrate prior and subsequent to the film deposition must be in exactly the same azimuthal directions. Otherwise, any slight change in the axis directions due to sample misalignment will significantly affect the measurement. A second difficulty is that even once reliable data is recorded, the modelling of it, although theoret-

* Corresponding authors. Fax: 44 1865 275410.
E-mail addresses: wuge.briscoe@chem.ox.ac.uk, wuge.briscoe@kau.se (W.H. Briscoe), robert.jacobs@chem.ox.ac.uk (R.M.J. Jacobs).
[1] Visiting scientist at Fakulteten för teknik- och naturvetenskap, Karlstad University, Universitetsgatan 1, SE65188 Karlstad, Sweden.
[2] Current address: Department of New Materials and Biosystems, Max-Planck-Institute for Metals Research, Heisenbergstr. 3, 70569 Stuttgart, Germany.
[3] Also at Department of Materials and Interfaces, Weizmann Institute of Science, Rehovot 76100, Israel.

0021-9797/$ – see front matter
doi:10.1016/j.jcis.2006.10.031

ically understood [7,8], is significantly more complex than for an isotropic material such as silicon. An alternative solution to this alignment issue in these optical methods would be to study the film deposition in situ, but the related practical difficulties have led to the common compromise in some previous studies, of using, e.g., a separate silicon substrate for ellipsometric characterisation of thin films while using mica for other types of analysis [9].

Over the past decades, grazing angle incidence X-ray reflectometry (XRR) [10–19] has been applied effectively to obtain information about nanofilm structures, and is a promising technique for mica substrates since its measurement is insensitive to mica birefringence. However, mica has hitherto been considered as a non-ideal substrate for the XRR technique [13] as explained below. In this letter, we report a simple "bending mica" method which enables the application of XRR to characterising different nanofilms on mica in air, using a table top X-ray reflectometer. Fitting the X-ray reflectivity curves with a simple layer-model using the standard Parratt algorithm allows us to extract the thickness and the apparent roughness of the nanofilms. Our method indicates how XRR may be extended as a useful characterisation tool for a wide range of nanofilms on mica.

2. Materials and methods

In our XRR measurements, which were performed using a Bruker® D8 reflectometer, a Cu$K\alpha$ X-ray beam (flux $\sim 10^6$ photons/s) of approximately 8 mm by 100 μm in cross section and wavelength $\lambda = 1.54$ Å is incident upon a sample at a grazing angle θ_i. This requires the sample to be flat over a few cm^2, and mica has been traditionally considered non-ideal for such measurements for two reasons. Firstly, a major difficulty arises from the inability to achieve sufficient flatness—a cleaved mica sheet undulates over such a large area. This results in the specular reflection ($\theta_i = \theta_r$) being spread over a range of detector angles (the range of which changes with incident angle), making it impossible to interpret the data. We have overcome this difficulty using a simple method, in which a freshly cleaved mica sheet of thickness $h = 30$–100 μm and ~4 × 4 cm (width b × length L) in size is gently bent and clamped onto an underlying cylinder ($R \sim 7.5$ cm; the geometry of the set-up is shown schematically at the top of Fig. 1). The enhanced rigidity of the mica sheet along the axis of bending is due to the very large stretching energy along this axis [20]. The *Searle parameter* for our mica sheets is $\mu = b^2/Rh \sim$ (210–710), and detailed analysis in the field of elasticity shows that bending deformation for such μ values falls into the "*plate regime*" [21], i.e., anticlastic bending (which would make the sheets bend into a saddle shape) is precluded along the apex of the axis, ensuring the flatness along this axis. Concomitantly, possible associated curvature effects can be alleviated by confining the detector cross section to 100 μm in height and 300–800 μm in width.[4] A set

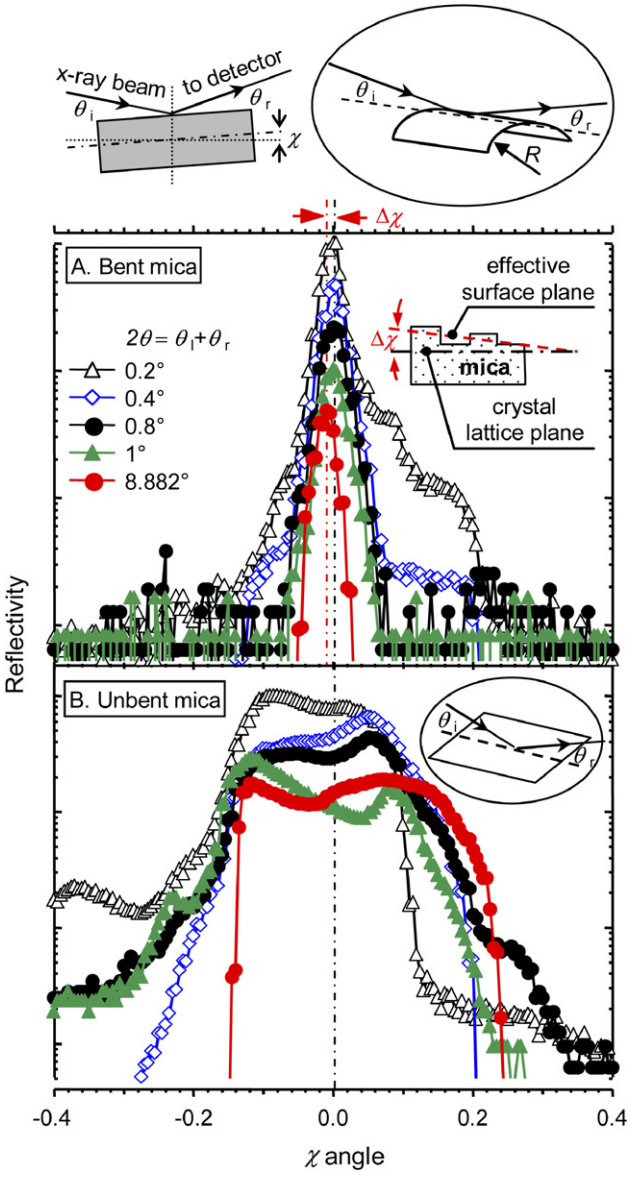

Fig. 1. Rocking curves (reflectivity in arbitrary units vs χ angle in degree on a log-liner scale) on bare mica in air using the bending mica method (A) in contrast to those using unbent mica (B), collected at different fixed total incident and reflection angles, $2\theta = \theta_i + \theta_f$. The reflectivity for each 2θ is obtained by normalizing the reflection counts with the maximum count; and thus the maximum reflectivity in each curve is 1 but an offset of 0.1 is added to different curves sequentially for clarity. The schematics at the top of the figure show the experimental set-up and the geometry of the bending mica method. The inset in (A) illustrates schematically the interpretation of the effective surface plane of reflection due to the presence of macroscopic domains on the mica surface, which gives rise to a small shift $\Delta\chi$ in the rocking curve taken at 2θ close to the Bragg angle.

of Soller slits on the detector side cuts out scattering that is more than 2° from the specular plane. The effectiveness of this method may be examined from the reflectivity "rocking curves" collected while fixing the total of the incident and reflection angles (i.e., $\theta_i + \theta_r = 2\theta$) and rocking the sample (i.e., varying the angle χ). Fig. 1A shows examples of such rocking curves measured on freshly cleaved bare mica in air, and the coincidence of the relative reflectivity peaks

[4] Thus, the incident and reflected beams are matched in size (100 μm) in the plane of specular reflection.

at different 2θ (0.2°–1°) indicates that the bent mica sheet is sufficiently flat to perform the grazing angle incidence XRR measurements.[5] This is in contrast to the poorly defined and broad peaks obtained on unbent mica shown in Fig. 1B—it would be impossible to interpret or analyse the XRR data from such an unbent mica substrate to generate any useful information.

A second reason why mica has been considered unsuitable for laboratory-based XRR measurements is that steps or terraces of height of order micrometer and lateral size of order millimeter to centimeter are inevitable over a large area on a cleaved mica sheet, giving rise to macroscopic domains—this is the so-called "mosaic effect" [13]. In theory, this may be tolerated because the large size of the domains, compared to the nanometer length scale of the nanofilms of interest, means they will not contribute coherently to specular reflection. In practice, however, it is as if the reflection takes place at an effective planar surface whose position is obtained by averaging over all the domains illuminated, and this effective plane is not necessarily parallel to the underlying mica lattices (as shown schematically in the inset to Fig. 1A). The rocking curve shown in red circles in Fig. 1A is collected at $2\theta = 8.882°$, where the reflectivity is dominated by the Bragg diffraction from the underlying mica crystal lattices. The small discrepancy in the reflectivity peak positions, $\Delta\chi \sim 0.01°$ in this case, is interpreted to be the angle between the effective surface plane of reflection and the crystal lattice plane. Such an interpretation could be further tested by examining the rocking curves collected at other 2θ angles (e.g., 2°–7°); however, due to the relatively low flux of our lab-based X-ray source, to obtain reliable reflectivity data at such high incident angles would have required extremely prolonged integration times. It should be noted that the presence of large numbers of small domains of these terraces could exaggerate the contribution of diffuse scattering to the specular reflection, an effect that could be exacerbated by the curved substrate geometry. In implementing our bending mica method, we have found it sufficient to avoid using mica sheets with too many small domains as judged by visual observations of reflected monochromatic light, and to keep the radius of curvature considerably larger than the beam footprint at the smallest angles studied.

Using this bending mica method, we have carried out proof-of-principle XRR measurements on three very different systems: (A) a Cr–Au nanofilm thermally evaporated in high vacuum on oxygen plasma-cleaned mica, (B) a surface-grown zwitterionic polymer brush made from poly(2-methacryloyloxyethyl phosphorylcholine) (pMPC) via atomic transfer radical polymerization from mica pre-initiated with an adsorbed random copolymer [22,23] and (C) a Langmuir–Blodgett (LB) monolayer of the phospholipid 1,2-dipalmitoylphosphatidylcholine (DPPC). The details for sample preparation and the AFM images of the samples are described in the supplementary material.

[5] The absence of Kiessig fringes in the diffuse reflectivity curves provides further evidence for the substrate flatness.

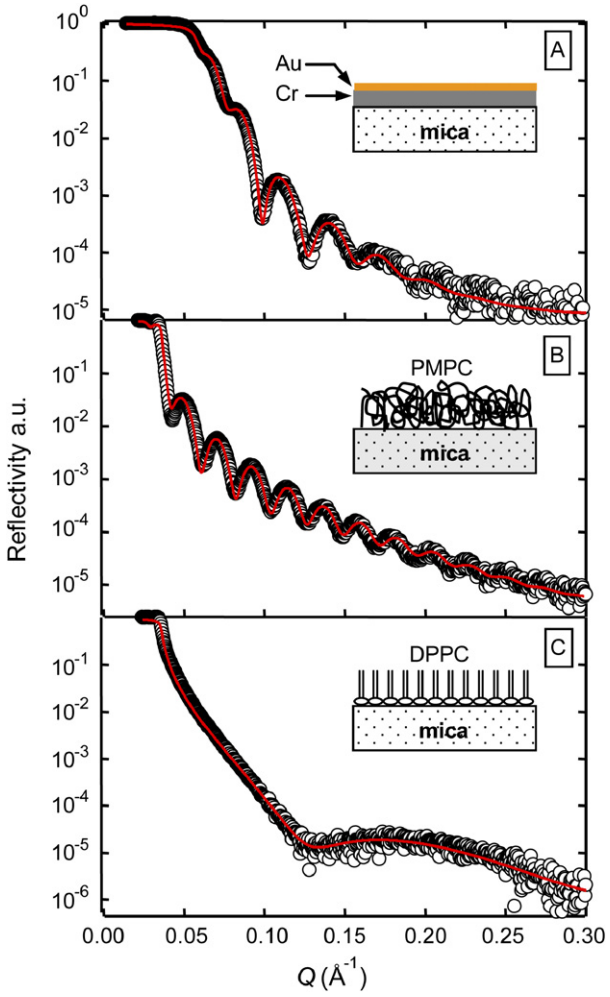

Fig. 2. Reflectivity vs momentum transfer $Q = (4\pi/\lambda)\sin\theta$ for three nanofilms on mica in air, as schematically illustrated in the insets: (A) ~5 nm Au and ~20 nm Cr thermally evaporated on plasma treated mica in high vacuum; (B) ~28 nm surface grown zwitterionic polymer brush pMPC; and (C) a ~2.5 nm DPPC phospholipid monolayer Langmuir–Blodgett deposited on mica. The open circles are the experimental data, and the red curves are computed using the fitting parameters listed in Table 1. The corresponding AFM images for these three nanofilms are shown in Fig. S2 in the supplementary material section.

3. Results and discussion

Fig. 2 shows reflectivity (open circles) vs $Q = (4\pi/\lambda)\sin\theta$ for these three nanofilms. Note the intensity fluctuations, known as Kiessig fringes, that arise from multiple beam interference in the presence of the nanofilms. In obtaining these reflectivity curves, we have first collected the specular reflection (i.e., $\theta_i = \theta_r$) and then subtracted from it the diffuse reflection (i.e., $\theta_r = \theta_i - \theta_{off}$) obtained over the same integration time to account for background scattering, with θ_{off} determined from rocking curves (see Fig. S1 in the supplementary material). The total acquisition time for both specular and off specular scans is typically around 24 h as 2θ varies between 0.1° and 5°. In addition, area corrections have been made at very small θ_i (below the critical edge $\theta_c \sim (2\delta)^{1/2}$) where the illumination area exceeds the sample size, knowing its relative reflectivity must be 1 due to total external reflection.

Table 1
Fitting parameters for different nanofilms using the Parratt algorithm: thickness t, real (dispersion) and imaginary (absorption) parts of the scattering length density SLD ρ_r and ρ_m, and apparent roughness σ

Samples	(A) Cr–Au			(B) pMPC			(C) DPPC	
Model	2 layer model			2 layer model			1 layer model	
Layers	Au	Cr	Bulk mica	pMPC layer	Macro-initiator under-layer	Bulk mica	Lipid layer	Bulk mica
t (Å)	50.2	193.4		260.4	16.0		25.7	
ρ_r (Å^{-2})	8.918e–05	5.922e–05	2.449e–05	1.125e–05	5.958e–06	2.579e–05	9.829e–06	2.539e–05
ρ_m (Å^{-2})	2.602e–06	7.649e–06	7.293e–07	5.329e–08	2.421e–07	7.368e–07	1.12e–07	9.94e–07
σ (Å)	25.0	13.8	6.0	9.3	1.8	4.4	5.0	5.7

In order to fit the Kiessig fringes in the reflectivity curves to extract structural information, we have used the simple layer model to describe the density profile of the nanofilms and the standard Parratt algorithm [10] to compute the reflectivity. The number of layers in the model is assigned first, biased by our knowledge of the nanofilm composition. Each layer is characterised by a complex index of refraction, $n = 1 - \delta + i\beta$, with δ and β respectively the dispersion and absorption terms, determined by the atomic composition of the layer and related to more commonly used complex scattering length density (SLD) $\rho = \rho_r + i\rho_m$ with $\rho_r = (2\pi/\lambda^2)\delta$ and $\rho_m = -(2\pi/\lambda^2)\beta$. The reflectivity is then computed recursively by varying the layer thickness t as well as n to fit the measured reflectivity curve. In the Parratt algorithm, the roughness amplitude σ at an interface is treated as the full width at half maximum (FWHM) of a Gaussian electron density variation across the interface, which causes a Debye–Waller-like damping of the reflection amplitude. Table 1 lists the four fitting parameters t, σ, ρ_r and ρ_m for each layer that we have used to compute the red curves in Fig. 2.

For the Cr–Au system (Fig. 2A), the fitted layer thicknesses are very close to those registered by the quartz crystal monitor during the sample preparation. The relatively large σ values at the air–Au and Au–Cr interfaces are consistent with the accepted picture of thin metallic film growth kinetics, according to which thermally evaporated metals should form islands at such a small thickness [24], and complementary atomic force microscope (AFM) imaging confirms the presence of island-like Au structures on the underlying Cr layer (Fig. S2). In the case of the surface-grown pMPC brush (Fig. 2B), we have found that a two-layer model gives a better fit than a one-layer model, with a surface layer accounting for the adsorbed initiating polymer layer underneath the pMPC brush. The fitted ρ_r is close to the theoretically predicted value based on the known SLD for pure MPC, suggesting a dense polymer layer and a collapsed brush conformation in air.[6] The corresponding AFM image (Fig. S2B) shows good surface coverage and nanometer scale surface roughness. The fitted ρ_r values for the Au, Cr, and the pMPC layers are physically reasonable in comparison to the theoretically calculated values, and consistent with the above interpretation of the nanofilm structures.

The Kiessig fringe from the thin LB DPPC monolayer spans over a larger Q range (Fig. 2C) and is more sensitive to background diffuse scattering. AFM imaging revealed the presence of pin holes in the lipid layer (Fig. S2C), which should lead to a reduced effective δ value. However, the fitted ρ_r of 9.829×10^{-6} Å^{-2} in Table 1 is higher than the theoretical value of 8.49×10^{-6} Å^{-2} for DPPC. This could be related to the Debye–Waller treatment of roughness which may be less appropriate in the case of the thin DPPC layer than other thicker films. It is possible that a more sophisticated model is needed to improve the fit [15,16], highlighting the intrinsic difficulty (i.e., on any substrate) with the XRR measurement on very thin nanofilms.

The fitted ρ_r values for mica for the three systems differ slightly from one another. This may be attributed to the active area correction and also the underlying errors in the measurement of the angle θ (thus within the scatter of the data).

In a pioneering study by Cheng et al. [26], synchrotron XRR was employed to examine the density oscillations of water adjacent to mica, and the authors acknowledged that such measurements on mica were nontrivial and required appropriate sample selection and mounting without elaborating on the details. The important features in their reflectivity curves were in a relatively high Q range (up to 5.6 Å^{-1}), implying a small X-ray beam footprint which could alleviate the demanding requirement for flatness in their mica sample. In a separate synchrotron study, Lee et al. [12] found it necessary to model the waviness in their free standing polymer films as a random distribution of lens shaped islands, in order to fit their XRR curves. We have demonstrated here that the bending mica method is effective in ensuring the flatness as required by the XRR measurement, and that the obtained reflectivity curves can be satisfactorily fitted using the simple layer-model to yield the film thickness and apparent roughness, at least in the case of the Cr–Au and pMPC nanofilms.

In summary, our main aim here is to demonstrate the practical usefulness of our simple bending mica method to facilitate XRR measurements of nanofilms. In doing so, we have chosen not to over-interpret our data, and hence used as simple a model as possible and fitted our data with the standard Par-

[6] It is likely that water has been incorporated in the pMPC layer. The scattering length densities of water and MPC are very similar, making it difficult to distinguish between them. We have ascertained the growth of the pMPC brush on mica by varying the polymerization time, which has resulted in different layer thicknesses. Further supporting evidence comes from our surface force measurements using an SFB [25].

rott algorithm that is readily available. We believe that such a simple layer model has satisfactorily described our data, and to our knowledge, this is the first report on XRR characterisation of nanofilms with mica as a substrate. Structural information of the type that we have obtained is particularly relevant to the direct force measurement techniques such as SFA/B and AFM that commonly employ mica as a model substrate. For instance, we have measured the surface forces and friction between pMPC brushes on mica using an SFA [23,25], and when compared with the dry pMPC brush thickness measured using XRR (Fig. 2B), our measurements give clear evidence that the brush swells significantly in aqueous media. The measurements presented here have been carried out using a laboratory-based X-ray reflectometer, the relatively low flux of which limits the surrounding medium to air. The much higher flux of a synchrotron X-ray source, and concomitantly its higher dynamic range, will enable such measurements to be extended to aqueous or organic liquid media.

Acknowledgments

The MPC monomer was kindly provided by Andrew Lewis (Biocompatibles®), and the ATRP macro-initiator by Steve Armes. The sample stage of the X-ray reflectometer was designed in part by Frank Schreiber. We would like to thank Simon Titmuss for his comments on our manuscript, and Susan Perkin and Robert Thomas for helpful discussions. Financial support from the EPSRC is gratefully acknowledged.

Supplementary material

(1) Sample preparations for the XRR measurement, (2) XRR rocking curves for the three nanofilm systems on mica, and (3) complementary AFM images of the three nanofilms. This material is available free of charge via the Internet at http://www.elsevier.com/.

DOI:10.1016/j.jcis.2006.10.031.

References

[1] J.N. Israelachvili, G.E. Adams, Nature 262 (1976) 774.
[2] J. Klein, Nature 288 (1980) 248.
[3] W.H. Briscoe, S. Titmuss, F. Tiberg, R.K. Thomas, D.J. McGillivary, J. Klein, Nature 444 (2006) 191.
[4] W.A. Ducker, T.J. Senden, R.M. Pashley, Nature 353 (1991) 239.
[5] P.I. Hanson, R. Roth, H. Morisaki, R. Jahn, J.E. Heuser, Cell 90 (1997) 523.
[6] R.P. Richter, A.R. Brisson, Biophys. J. 88 (2005) 3422.
[7] J. Lekner, Theory of Reflection, Martinus Nijhoff Publishers, Dordrecht, 1987.
[8] M. Born, E. Wolf, Principles of Optics Electromagnetic Theory of Propagation Interference and Diffraction of Light, sixth ed., Cambridge Univ. Press, Cambridge, 1999.
[9] P.M. Claesson, E. Blomberg, O. Paulson, M. Malmsten, Colloids Surf. A 112 (1996) 131.
[10] L.G. Parratt, Phys. Rev. 95 (1954) 359.
[11] M. Schalke, M. Losche, Adv. Colloid Interface Sci. 88 (2000) 243.
[12] D.R. Lee, K. Shin, O.H. Seeck, H. Kim, Y.S. Seo, M. Tolan, M.H. Rafailovich, J. Sokolov, S.K. Sinha, Phys. Rev. Lett. 90 (2003).
[13] P. Fenter, in: P. Fenter, M. Rivers, N.C. Sturchio, S. Sutton (Eds.), Applications of Synchrotron Radiation in Low-Temperature Geochemistry and Environmental Science, in: Reviews in Mineralogy and Geochemistry, vol. 49, Geochemical Society, 2002, p. 149.
[14] R.K. Chew, S.F. Yoon, H.K. Chan, C.F. Ng, Q. Zhang, J. Ahn, Int. J. Mod. Phys. B 16 (2002) 1072.
[15] P. Poloucek, U. Pietsch, T. Geue, Ch. Symietz, G. Brezesinski, J. Phys. D Appl. Phys. 34 (2001) 450.
[16] E. Politsch, G. Cevc, J. Appl. Crystallogr. 35 (2002) 347.
[17] A.S. Brown, S.A. Holt, P.M. Saville, J.W. White, Aust. J. Phys. 50 (1997) 391.
[18] J. Als-Nielsen, D. McMorrow, Elements of Modern X-Ray Physics, Wiley, West Sussex, UK, 2001.
[19] M. Tolan, X-Ray Scattering from Soft-Matter Thin Films, Springer, Heidelberg, 1999.
[20] A. Boudaoud, P. Patricio, Y. Couder, M. Ben Amar, Nature 407 (2000) 718.
[21] S.K. Kaldor, I.C. Noyan, Appl. Phys. Lett. 80 (2002) 2284.
[22] X.Y. Chen, S.P. Armes, Adv. Mater. 15 (2003) 1558.
[23] M. Chen, W.H. Briscoe, S.P. Armes, H. Cohen, J. Klein, J. Am. Chem. Soc. (2006), submitted for publication.
[24] D.W. Pashley, M.J. Stowell, M.H. Jacobs, T.J. Law, Philos. Mag. 10 (1964) 127.
[25] M. Chen, W.H. Briscoe, J. Klein, 2006, in preparation.
[26] L. Cheng, P. Fenter, K.L. Nagy, M.L. Schlegel, N.C. Sturchio, Phys. Rev. Lett. 8715 (2001).